Atmospheric Environment 318 (2024) 120235

Contents lists available at ScienceDirect

Atmospheric Environment

journal homepage: www.elsevier.com/locate/atmosenv

# Comparison of secondary organic aerosol (SOA)-associated molecular features at urban sites in China and Korea in winter and summer (2019)

Min Sung Kim [a,b], Yujue Wang [c,1], Mira Choi [a], Shiyi Chen [c], Min-Suk Bae [d], Kihong Park [e], Min Hu [c,**], Kyoung-Soon Jang [a,f,*]

[a] Bio-Chemical Analysis Team, Korea Basic Science Institute, Cheongju, 28119, Republic of Korea
[b] Department of Environmental Engineering, Yonsei University, Wonju, 26493, Republic of Korea
[c] State Key Joint Laboratory of Environmental Simulation and Pollution Control, College of Environmental Sciences and Engineering, Peking University, Beijing, 100871, China
[d] Department of Environmental Engineering, Mokpo National University, Muan, 58554, Republic of Korea
[e] School of Earth Sciences and Environmental Engineering, Gwangju Institute of Science and Technology, Gwangju, 61005, Republic of Korea
[f] Division of Bio-Analytical Science, University of Science and Technology, Daejeon, 34113, Republic of Korea

## HIGHLIGHTS

- A total of 10,790 chemical formulas assigned from $PM_{2.5}$-drived WSOC samples.
- SOC fractions were discriminated from the WSOC compositions.
- SOC compounds during winter in Gwangju exhibit a more aliphatic nature than in Beijing.
- Gwangju exhibit a more favorable environment for SOA formation process than Beijing.

## GRAPHICAL ABSTRACT

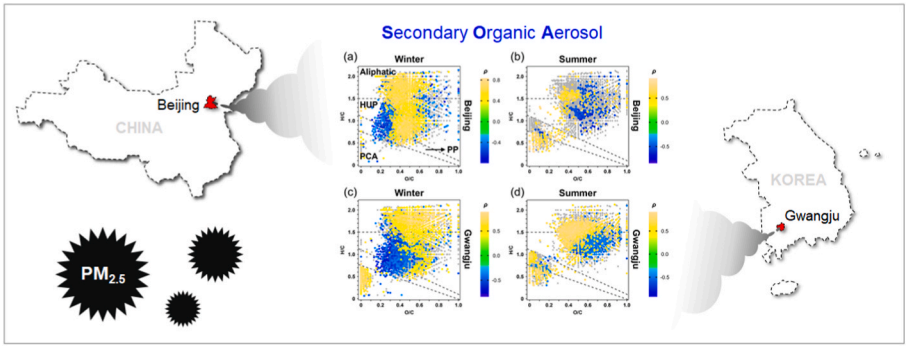


## ARTICLE INFO

*Keywords:*
$PM_{2.5}$
FT-ICR MS
Secondary organic carbon
SOA formation
Molecular feature
Stagnant condition

## ABSTRACT

Secondary organic aerosol (SOA) formation is important in the field of atmospheric science due to its impacts on public health and climate change. However, the molecular compositions or formation mechanisms of SOA have not been fully characterized in ambient atmospheres. In this study, ambient fine particle ($PM_{2.5}$) samples were collected in two urban cities in Beijing, China and Gwangju, Korea during the winter and summer seasons, and the SOA-associated molecular features were characterized by using Fourier transform-ion cyclotron resonance mass spectrometry (FT-ICR MS). We found that the secondary organic carbon (SOC) during wintertime in Gwangju exhibit a more aliphatic nature, and those in Beijing have more aromatic structures like humic compounds. The contribution of CHOS to the total identified WSOC associated SOC was the most abundant at Beijing

* Corresponding author. Bio-Chemical Analysis Team, Korea Basic Science Institute, Cheongju, 28119, Republic of Korea.
** Corresponding author.
*E-mail addresses:* minhu@pku.edu.cn (M. Hu), ksjang@kbsi.re.kr (K.-S. Jang).
[1] Present address: Frontiers Science Center for Deep Ocean Multispheres and Earth System, Key Laboratory of Marine Environment and Ecology, Ministry of Education of China, Ocean University of China, Qingdao 266,100, China.

https://doi.org/10.1016/j.atmosenv.2023.120235
Received 18 July 2023; Received in revised form 14 October 2023; Accepted 20 November 2023
Available online 24 November 2023

site (~40%) compared to the Gwangju site (~30%), and the proportion of CHON species in the WSOC associated SOC accounted for ~30% in Beijing and 20–30% in Gwangju. Majority of SOC-derived CHOS species (~99%) likely contained sulfate functional groups at both sites regardless of the sampling season. Organonitrates predominated in CHON species in summer compared to winter, but some fractions appeared to contain other potential nitrogen functional groups such as amide and nitrile (~20%), suggesting the existence of other formation pathways of organic nitrogen, especially during winter. This work gave an observation insight into the molecular features of SOC at two different sites, and will deepen the understanding on the region-specific SOA formation mechanisms.

## 1. Introduction

Organic aerosols (OAs) account for up to 50% of the total mass of ambient fine particles (Heintzenberg, 1989; Huang et al., 2014; Jimenez et al., 2003; Seinfeld and Pandis, 2016) and have been gaining increasing attention due to their impacts on air quality, climate change and human health (Poschl, 2005). Atmospheric OAs are comprised of primary organic aerosols (POAs), which are generated by fossil-fuel combustion, biomass burning, traffic, and industrial processes and directly emitted into the atmosphere, and secondary organic aerosols (SOAs), which are mainly formed from the chemical transformation of primary atmospheric organic compounds, such as oxidation of gaseous volatile organic compounds (VOCs) (Hallquist et al., 2009; Kroll and Seinfeld, 2008; McNeill, 2015; Poschl, 2005). The molecular composition of SOA and the formation mechanism have received the most attention because they can be used to elucidate source origins, aging mechanisms and transformation processes, and SOA formation is closely related to the occurrence of haze episodes in urban areas (Han et al., 2017; Li et al., 2020; Wang et al., 2021; Zheng et al., 2021).

The carbonaceous components of OAs can be divided into organic carbon (OC) and elemental carbon (EC), and EC is known to absorb solar radiation, thus contributing to warming the atmosphere (Bond et al., 2013) and OC has been considered to counteract global warming owing to its solar radiation scattering properties (Kasper-Giebl et al., 1999). In particular, atmospheric fine particle ($PM_{2.5}$)-derived water-soluble organic carbon (WSOC) fraction is generally thought to be associated with the hygroscopic growth of aerosols, cloud condensation nuclei (CCN) activity and cloud droplet formation, and the scattering of the solar radiation (Matsumoto, 2022). WSOC also plays a significant role in the atmospheric transformation of primary organic molecules mainly due to their hygroscopic properties, which can determine their physicochemical properties including the size, concentration, and phase state of aerosols (Jing et al., 2016). In addition, the WSOC fraction is considered to include SOA formation products [that is, secondary organic carbon (SOC)], so a deeper understanding of the molecular compositions of $PM_{2.5}$-carried WSOC is needed to unveil the SOA formation pathways and their potential impacts on climate change and public health. However, detailed information on the SOC constituents and the formation mechanism is still lacking due to the complexity and diversity of the components and the environments, depending on local sources, meteorological conditions, and the related atmospheric chemistry (Seinfeld and Pankow, 2003; Turpin et al., 2000).

Recently, several SOA formation and/or aging mechanisms have been proposed by smog chamber experiments, which can provide a more controlled environment (i.e., concentrations of precursors or catalysts, temperature or humidity) and less complicated products for simulating certain atmospheric reactions of interest than the actual atmosphere (Babar et al., 2016; Chuang and Donahue, 2017; Jorga et al., 2020; Liu et al., 2015; Qi et al., 2020). Qi and colleagues showed the effects of nitrogen oxides (NOx) on SOA formation from the photooxidation of toluene and ammonia for the chemical aging of toluene SOA using a smog chamber study (Qi et al., 2020). Mayorga and coworkers demonstrated that the nitrate radical oxidation of phenolic VOCs is one of the ways to produce secondary organic aerosols, thereby generating organonitrate compounds in laboratory experiments (Mayorga et al., 2021). Although those smog chamber studies demonstrated some SOA formation mechanisms and the contributions of certain precursors or catalysts (Babar et al., 2016; Liu et al., 2015), there is a large portion of uncertainty between field measurements and chamber experiments due to the complexity of the formation pathway of SOAs in the ambient atmosphere, and the details and related products in field samples have not yet been fully studied. For example, there are several chemical simulation models for SOA formation available, mainly based on coefficients derived from smog chamber experiments (Chung and Seinfeld, 2002; Hoffmann et al., 1997; Tsigaridis and Kanakidou, 2003); however, many uncertainties in the SOA formation processes, such as higher concentrations of precursors, sticking coefficients of semi-VOCs, enthalpy of vaporization of compounds of interest, dimer or oligomer formations in the aerosol phase, that can be happened in real atmospheric conditions (Olcese et al., 2007). To close the gap between the laboratory and field conditions, Jorga and colleagues used a dual smog chamber system filled with ambient air, but nitrous acid was added only to the perturbed chamber (Jorga et al., 2020). Using the dual smog chamber system, they were able to quantify the formation rates of SOAs (i.e., organic tracers and inorganic species including nitrate and sulfate) under noon-time OH concentrations in ambient air.

Ultrahigh-resolution Fourier transform-ion cyclotron resonance mass spectrometry (FT-ICR MS) has been widely utilized as a powerful tool for elucidating the molecular details of complicated organic constituents, which can be isolated from various environmental and biological samples, such as water, soils, cell media, and/or aerosols (Bianco et al., 2019; Ksionzek et al., 2016; Wozniak et al., 2008; Zhou et al., 2020). In particular, the molecular level characterization of aerosol-derived organic constituents was performed to elucidate the molecular composition in detail. Wozniak and coworkers demonstrated the molecular composition of WSOC from aerosol samples, and presented SOC-related compounds in van Krevelen diagrams (region with $0.2 < O/C < 0.7$ and $0.8 < H/C < 1.5$) (Wozniak et al., 2008). These criteria were suggested empirically by observations based on laboratory investigations (Altieri et al., 2008; Reinhardt et al., 2007), but those were not sufficient to discriminate SOA components from OA profiles. There are few reports that can show SOA-related chemical/molecular constituents and their formation mechanisms. Although high-resolution MS profiles of aerosol-derived organic substances could provide highly sophisticated chemical and molecular information on the organic compositions, it might get confused from the information without any reliable criteria on the SOA-related features. Therefore, another criterion to demonstrate SOA-associated molecular features in the massive amount of molecular information is needed as a breakthrough.

While indeed there may be various sources contributing to WSOC, the preeminent ones recognized within the scientific community are direct emissions from biomass burning and the formation of SOA. This recognition is substantiated by previous research works (Decesari et al., 2006; Jin et al., 2020; Saxena and Hildemann, 1996), which have consistently identified these as the most significant contributors to WSOC. In some instances, field studies have unveiled WSOC predominantly originating from secondary sources, thereby positioning it as a valuable proxy for SOA, especially in regions that lack prominent biomass burning influences (Kondo et al., 2007; Weber et al., 2007). Feng and colleagues demonstrated that the estimation of SOCs using a

WSOC-based method was more reliable than EC-based or tracer-based methods (Feng et al., 2013). Although other sources such as coal combustion, dust and vehicle emissions could contribute to WSOC, it was assumed here that WSOC is primarily associated with SOA formation and/or biomass burning. Biomass burning-related WSOC ($WSOC_{BB}$) is calculated from the ratio of levoglucosan to OC, and then, nonbiomass burning-related WSOC ($WSOC_{NBB}$) can be determined by differences between total WSOC and $WSOC_{BB}$, resulting in the relative contribution of primary organic carbon (POC) and SOC to the measured OC values of airborne particles. In our previous report, the estimation of SOC concentrations was also used to investigate the relationships with VOCs and $NH_3$ in agricultural areas (Song et al., 2021). Using the estimated SOC concentrations, it would be expected to figure out the correlation with individual molecular features of WSOC, extracting the SOC-responsive molecular features from the entire WSOC compositions.

Air pollutants do not adhere to geopolitical boundaries; rather, they traverse vast distances, making air pollution a challenge that necessitates collaboration among neighboring nations. Therefore, international efforts have gained prominence, with multiple collaborative research initiatives emerging to tackle environmental issues on a global scale (Arimoto et al. 1996, 2004; Choi et al., 2019a; Crawford et al., 2021; Halliday et al., 2019; Hoell et al., 1996; Park et al., 2021; Peterson et al., 2019; Topping et al., 2004). One such noteworthy endeavor is the joint Korea-China campaign, supported by the National Research Foundation of Republic of Korea (NRF) and carried out from 2017 to 2020, known as the $PM_{2.5}$ Research Project. This groundbreaking research initiative sought to elucidate the chemical composition of atmospheric $PM_{2.5}$, shedding light on the sources and mechanisms behind haze episodes occurring in two distinct yet interconnected regions: Gwangju, South Korea, and Beijing, China, as demonstrated in our previous reports (Jang et al., 2020; Oh et al., 2023; Park et al., 2020). Beijing, as the capital city of China, notably faced severe episodes of smog and haze until 2013. The Chinese government, in recognition of the gravity of the situation, initiated the Air Pollution Prevention and Control Action Plan (APPCAP) in 2013. The implementation of this comprehensive action plan heralded a marked improvement in air quality in the region (Guo et al., 2018; Liu et al., 2023; Wang et al., 2023; Yang et al., 2020). Gwangju, on the other hand, ranks as the 6th largest city in South Korea and is located in a northwest wind trajectory from Beijing. Although both cities share common attributes in terms of their urban environments, including agricultural, residential, commercial areas, and major highways, they diverge significantly in terms of meteorological conditions (Park et al., 2020). These differences encompass factors such as wind speed, temperature, and relative humidity. According to the chemical composition analysis and source apportionment results of our previous report (Park et al., 2020), a combination of multiple primary combustion sources and secondary formation under stagnant conditions and dusts under high wind speeds were the main contributors to haze episode at Beijing site, while Gwangju was more influenced by secondary formation of nitrate and organics under stagnant conditions. Consequently, it becomes evident that the characterization of air pollutants in both regions is indispensable to gain a comprehensive understanding of their sources and the intricate mechanisms that underlie their formation.

In the present study, ambient $PM_{2.5}$ were collected simultaneously in two urban cities in China and Korea (Beijing and Gwangju, respectively) during the winter and summer of 2019, and WSOC fractions of the $PM_{2.5}$ samples were investigated using ultrahigh-resolution Fourier transform ion cyclotron resonance mass spectrometry (FT-ICR MS) to acquire detailed molecular features. SOC fractions can be discriminated from the fractions of biomass burning in the FT-ICR MS-derived WSOC datasets using Spearman rank correlation analysis with the POC and SOC indices. We also determined the differences in the SOC-associated molecular features in different regions in winter and summer, which will provide new insights to understand the region-specific SOA formation mechanisms.

## 2. Materials and methods

### 2.1. Sampling of ambient fine particles ($PM_{2.5}$)

Ambient fine particles ($PM_{2.5}$) were collected simultaneously at 24 h intervals in Beijing and Gwangju during winter (27 December 2018–25 January 2019, 30 samples in each site) and summer (5–23 August 2019, 19 samples in each site), respectively. Daily sampling times were 09:00–08:30 (next day) at the Beijing site and 10:00–09:30 (next day) at the Gwangju site. In total, 98 samples were obtained from both sites during the sampling period. Sampling at the Beijing site was performed on the roof of a building on the Changping campus of Peking University (40.14°N, 116.11°E), 38 km northeast of urban Beijing. The Changping area is known to be highly influenced by biomass burning and vehicle emissions from neighboring settlements and the urban area of Beijing during winter (Zhang et al., 2018). The Gwangju site was located on the roof of the Gwangju Institute of Science and Technology (35.13°N, 126.50°E). This site is located north (~8 km) of downtown Gwangju, where it is affected by a variety of pollution sources from agricultural areas, residential and commercial areas, industry, and highways, including biomass burning, heating, cooking, and industrial and traffic emissions (Lee et al., 2018).

### 2.2. Preparation of WSOC from $PM_{2.5}$ samples

The fraction of WSOC was extracted from the $PM_{2.5}$ samples (ca. 6 $cm^2$ of quartz filters) by placing the samples in ultrapure water and ultrasonicating the solution for 60 min at room temperature, as previously described (Jang et al., 2019). The temperature of the ultrasonic bath was maintained at approximately 25 °C by continuously circulating tap water. The $PM_{2.5}$ mass per corresponding filter area ranged from 0.21 to 3.18 mg for the winter season and 0.11–1.19 mg for the summer season. Before extraction, 50 μL of 5-bromo-3-iodo-7-azaindole (100 μg $mL^{-1}$) was added to the solutions as an internal standard for internal calibration during sample measurements and signal normalization during data processing. The extracts were subjected to filtration using a glass syringe with a 0.45 μm Teflon filter to remove insoluble debris, and then, the filtrates were solid-phase extracted using a 3 mL Bond Elut PPL cartridge (Agilent, Santa Clara, CA). Briefly, the PPL cartridges were precleaned by passing them through 6 mL methanol, and then, they were conditioned with 6 mL 0.1% formic acid in water. Ten milliliters of the samples were loaded into the PPL cartridge, followed by washing with 6 mL of ultrapure water. The WSOC fractions retained in the cartridges were eluted with methanol. The eluate was dried under a nitrogen stream. Then, the dried samples were analyzed using an FT-ICR mass spectrometer after being reconstituted with 100 μL of 50% (v/v) aqueous acetonitrile. Highly pure HPLC-grade solvents were used in this study (i.e., 99.9% for methanol and acetonitrile). A field blank filter extract was also prepared in the same manner as a control.

### 2.3. FT-ICR MS analysis and data processing for elemental formula assignment

Highly accurate mass measurements of WSOC samples were carried out with FT-ICR MS (solariX XR™ system, Bruker Daltonics, Bremen, Germany) equipped with a 15 T superconducting magnet and a standard electrospray ionization (ESI) interface (Apollo II, Bruker Daltonics), as demonstrated previously (Jang et al., 2019). The WSOC extracts were directly infused into the mass spectrometer at a flow rate of 2 μL $min^{-1}$ using a syringe pump. The MS was externally calibrated using a NaTFA solution (100 μg $mL^{-1}$ in methanol) with calibration errors below 0.1 ppm before sample measurement. The FT-MS spectra for the samples were recorded from $m/z$ 150 to 1200 with 100 scans per spectrum in negative ion mode with a time-domain transient of 4 mega words size and phase-corrected with the absorption mode, thereby yielding a resolving power of 800,000 (FWHM at $m/z$ 400). The optimal conditions

of FT-ICR MS analysis were as follows: a capillary voltage of 3.5 kV, the drying gas flow of 4 L $min^{-1}$, the drying gas temperature of 200 °C, the ion accumulation time of 0.05 s, the transient length of 2.79 s, and the time of flight of 0.7 s for all experiments.

The FT-ICR MS datasets were subjected to further processing, including peak detection and recalibration, using DataAnalysis (ver. 4.4, Bruker Daltonics) and elemental formula assignment using Composer (Sierra Analytics, Modesto, CA). Briefly, the empirical molecular formulas were determined for the masses of singly charged ions in the range of $m/z$ 150–1000 by combinations of $C_{1-100}H_{1-200}O_{1-60}N_{0-4}S_{0-2}$, and then, the molecular formulas with assignment errors >0.3 ppm were excluded from further interpretation. The assigned chemical compositions were displayed based on the atomic hydrogen-to-carbon (H/C) and oxygen-to-carbon (O/C) ratios on a van Krevelen diagram (Kim et al., 2003). The modified aromaticity index ($AI_{mod}$) was used to interpret the aromaticity of organic molecules (Koch and Dittmar 2006, 2016). The double bond equivalent (DBE) value, representing the sum of rings and double bonds in each molecule, can be calculated from the number of atoms in the chemical formulas by the following equation: $DBE = 1 + C - 0.5\,H + 0.5\,N$. The nominal oxidation state of carbon ($OS_C$) was calculated by the following equation: $OS_C = 4 - [4 + H/C - 3\,N/C - 2O/C - 2S/C]$. Organic constituents can be categorized into four chemical classes based on their elemental composition [i.e., compounds containing only C, H and O (CHO), compounds containing C, H, O and N (CHON), compounds containing C, H, O and S (CHOS), and compounds containing C, H, O, N and S (CHONS)] (Choi et al., 2019a). The proportion of each compound group was estimated based on the FT-ICR MS peak-intensity-weighted percentage of the total.

The assigned molecular formulae were classified into five subgroups based on their $AI_{mod}$ and H/C ratio that can reflect the structures of aromatic rings and aliphatic chains of certain compound: (1) polycyclic condensed aromatics (CA); $AI_{mod} > 0.66$, (2) polyphenolic (PP); $0.5 < AI_{mod} \leq 0.66$, (3) highly unsaturated and phenolic (HUP); $AI_{mod} \leq 0.5$; $H/C < 1.5$, (4) aliphatic; $AI_{mod} \leq 0.5$ and $1.5 \leq H/C < 2.0$ (Coward et al., 2019).

### 2.4. WSOC-based estimation of SOC and POC concentrations

According to the previous literature by Feng et al. (2013), the concentrations of SOCs in the $PM_{2.5}$ samples were estimated by using a WSOC-based method. Given this assumption that the molecular constituents of the WSOC fraction are primarily associated with SOA formation or biomass burning (Kondo et al., 2007; Weber et al., 2007), the biomass burning-related WSOC ($WSOC_{BB}$) was calculated from the ratio of levoglucosan to OC [Equation (1)], and the nonbiomass burning-related WSOC ($WSOC_{NBB}$) was determined by differences between total WSOC and $WSOC_{BB}$ [Equation (2)], as described in the publications (Feng et al., 2013; Oh et al., 2018; Song et al., 2021).

$$WSOC_{BB} = \frac{WSOC_{BB}}{OC_{BB}} \times \frac{OC_{BB}}{Levoglucosan_{BB}} \times Levoglucosan \quad \text{[Equation (1)]}$$

$$WSOC_{NBB} = WSOC_{Total} - WSOC_{BB} \quad \text{[Equation (2)]}$$

The value of $WSOC_{BB}/OC_{BB}$ was calculated as 0.70 from the literature by Sannigrahi et al. (2006). In particular, levoglucosan stands as a paramount organic tracer for biomass burning aerosols within the Earth's atmosphere, renowned for its effectiveness in this regard. It is worth noting, however, that the measured ratio of levoglucosan to organic carbon ($Levog_{BB}/OC_{BB}$) can exhibit variability contingent on factors such as sampling location and season. Moreover, this ratio is inherently influenced by combustion conditions and the specific type of biomass being burned, rendering the precise estimation of such ratios for a given region and season a rather formidable challenge. In pursuit of a comprehensive understanding, our study has systematically referenced fifteen distinct $Levog_{BB}/OC_{BB}$ values originating from diverse biomass combustion experiments, meticulously curated from five prior research works (Calvo et al., 2015; Fine et al., 2001; Gonçalves et al., 2011; Puxbaum et al., 2007; Salma et al., 2017) (see Supplementary Table S2). Through an intricate synthesis of this wealth of data, we have derived an average $Levog_{BB}/OC_{BB}$ value gleaned from previous research endeavors, which collectively encompass a wide spectrum of wood combustion experiments. This average, calculated to be 0.24, holds significant implications for our study, further yielding an $OC_{BB}/Levog_{BB}$ ratio of 4.17. Here, the $WSOC_{NBB}$ concentration corresponds to the SOC concentration, and the POC concentration is finally determined by subtracting the SOC from OC.

### 2.5. Multivariate statistical analysis

Canonical correspondence analysis (CCA) is a multivariate ordination technique that determines axes from the response data as a linear combination of measured predictors. In ecology, CCA is often used to extract gradients that drive the composition of ecological communities (ter Braak and Verdonschot, 1995). Therefore, it can elucidate the relationship between two sets of data such as microbial species abundance at different sites and environmental variables on the same sites. That is, CCA uses two different data sets to describe relationships between variables, compared to principal component analysis (PCA), which uses one data set (i.e., microbial abundance) to describe differences in community composition between samples. In this study, CCA was used to visualize the difference in the chemical compositions of WSOC fractions collected from Beijing and Gwangju using the mean intensity of each formula along with their relationships with environmental variables. The normality of variables was tested by the Shapiro–Wilks test for all variables. All steps were computed in R applying the 'vegan' package (Oksanen et al., 2014); especially, CCA was performed with the 'cca' function of the 'vegan' package, and the correlation test was conducted using the 'stats' package (R Core Team, 2020). Pearson's correlation between the proportion of molecular classes and chemical compositions was calculated.

To determine how the indices of POC and SOC were associated with WSOC chemical composition, Spearman's rho was calculated between the indices and the relative abundances of individual molecular formulas for all the samples. Spearman's rho was visualized in a heatmap and a van Krevelen diagram for each module, and only formulas with Spearman's rho >0.4 were presented in the van Krevelen diagram to simplify the plot.

### 2.6. Air mass transport analysis

The air mass backward trajectories of a given air mass arriving at the sampling sites were calculated to estimate the air mass transport history using the Hybrid Single-Particle Lagrangian Integrated Trajectory (HYSPLIT) model of the National Oceanic and Atmospheric Administration (NOAA) and meteorological data from the Global Data Assimilation System (GDAS) of the National Centers for Environmental Information (NCEI) database (Draxler and Hess, 1998). The 72-h backward air mass trajectories were computed in 3-h intervals using the HYSPLIT model with an endpoint height of 100 m at the receptor site, as described in our previous studies (Choi et al., 2019a; Park et al., 2020). In total, 704 air mass backward trajectories were obtained during the sampling periods (winter: 480; summer: 304, respectively). To categorize the major air masses affecting the receptor sites, air mass backward trajectory data were clustered using an angle-based distance matrix, taking into account the distance between each pair of back trajectories (Bogawski et al., 2019; Sirois and Bottenheim, 1995). All computation steps were run in R using openair packages (Carslaw and Ropkins, 2012; R Core Team, 2020).

## 3. Results and discussion

### 3.1. Molecular characterization of WSOC in $PM_{2.5}$ collected during winter and summer seasons at Beijing and Gwangju sites

The daily mean $PM_{2.5}$ concentrations at Beijing and Gwangju during the winter period were substantially higher (33.65 μg $m^{-3}$ and 32.34 μg $m^{-3}$, respectively) than those during the summer period (20.24 μg $m^{-3}$ and 20.03 μg $m^{-3}$, respectively). The temporal distributions of the 24-h averaged $PM_{2.5}$ concentrations at the two sampling sites showed no significant difference ($p = 0.99$ for winter and $p = 0.74$ for summer) throughout the sampling periods (see Supplementary Fig. S1). In this study, we aimed to elucidate the compositional difference of SOC collected at different sites and different seasons, so ultrahigh-resolution FT-ICR MS analysis was performed to figure out molecular level differences on the compositions of the $PM_{2.5}$-carried WSOC.

A total of 10,790 chemical formulas were assigned from $PM_{2.5}$-derived WSOC samples at the Beijing and Gwangju sites by high-resolution ESI (−) FT-ICR MS measurements. The majority of the molecular formulae of WSOC in Beijing during wintertime was dominated by the CHOS group (25.5–40.1%, mean = 33.3% ± 3.5%), while at the Gwangju site the CHONS (15.5–40.1%, mean = 33.8% ± 7.2%) and CHOS (22.1–39.3%, mean = 29.4% ± 3.9%) accounted for 63.1%, in all samples (Fig. 1 and see Supporting Information). The majority of the molecular formulae in Beijing during summertime were CHONS (6.9–45.2%, mean = 33.8% ± 11.7%), while at the Gwangju site the CHONS (17.6–62.3%, mean = 41.1% ± 10.7%) was dominated, respectively. According to the van Krevelen diagrams of WSOC fractions in $PM_{2.5}$ samples (Fig. 1), WSOC during the winter apparently seemed to exhibit less aliphatic nature (lower H/C ratio) and less oxidized state (lower O/C ratio) than those during the summer. The higher H/C and O/C ratios of WSOC during the summer were agreed well with previous observations (Kondo et al., 2007; Ning et al., 2022; Trump and Donahue, 2014) and probably support the attribution to SOC formation processes leading to aliphatics and highly unsaturated structures. Besides, no significant correlation was observed between each fractions of chemical class compounds in WSOC and representative secondary inorganic ions (i.e., nitrate and sulfate) (Supplementary Fig. S2).

We conducted a canonical correspondence analysis (CCA) including all elemental formulas assigned from all WSOC samples, gaseous species, particulate ions, and meteorological conditions encompassing temperature (Temp) and relative humidity (%RH) (Fig. 2 and Supplementary Fig. S3). The first two axes, CCA1 and CCA2, explained 45.2% and 15.6% for winter and 38.8% and 16.9% for summer, respectively, of the variability of WSOC-related indices. During the winter, the WSOC samples from Beijing and Gwangju were clearly separated by CCA1 ordination. Temp, %RH, and $O_3$ showed positive CCA1 loadings, while $SO_2$ and CO displayed negative CCA1 and positive CCA2 loadings (Fig. 2a), i.e. CCA1 was closely and positively associated with haze events at the Gwangju site, supporting Temp and %RH were the main drivers for WSOC composition in Gwangju, and $SO_2$ and CO significantly contributed for the attribute of WSOC in Beijing. During the summer, WSOC samples from both Beijing and Gwangju sites were less obviously clustered than the winter clustering (Fig. 2b). Temp and $SO_2$ were the representative of positive CCA1 loadings, and $NO_2$, $NO_3^-$ and $O_3$ showed negative CCA1 loading. Given these observations, the wintertime samples were well clustered by each region compared to those from the summer season, likely implying that the molecular composition of

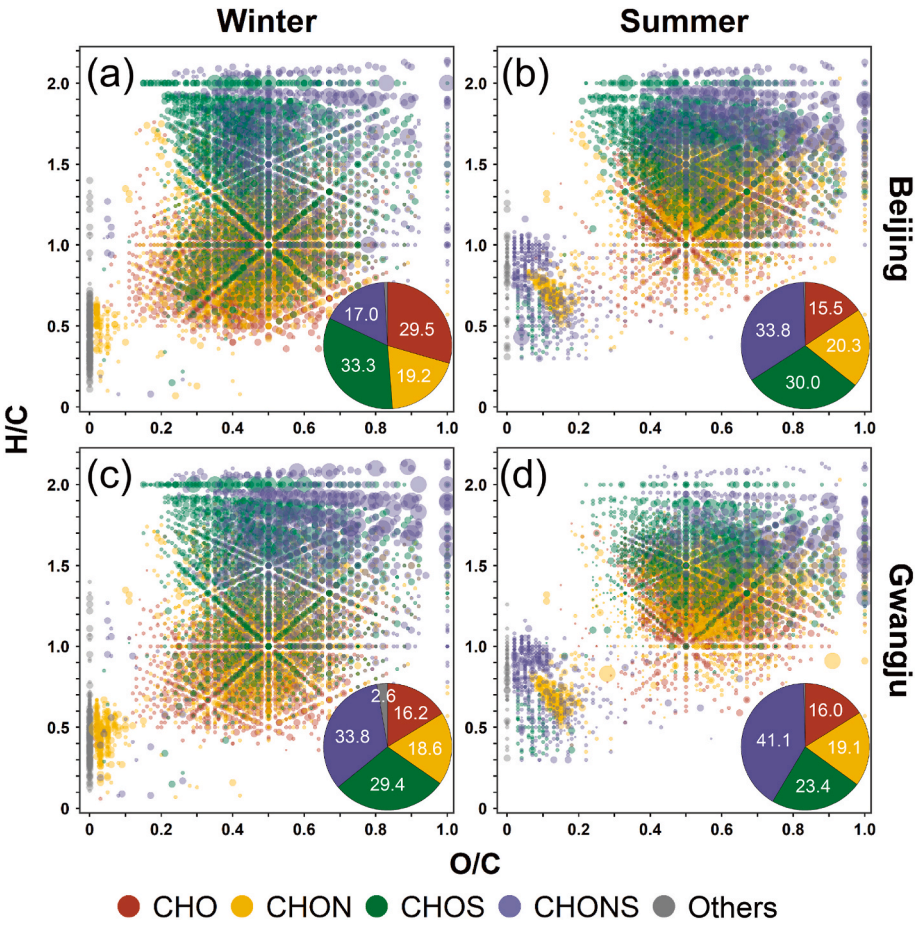


**Fig. 1.** Van Krevelen plots of the assigned chemical formulas in the $PM_{2.5}$-derived WSOC: the (a) winter and (b) summer observations in Beijing, and the (c) wither and (d) summer observations in Gwangju. The pie charts show the relative contributions of each chemical group in terms of peak intensity.

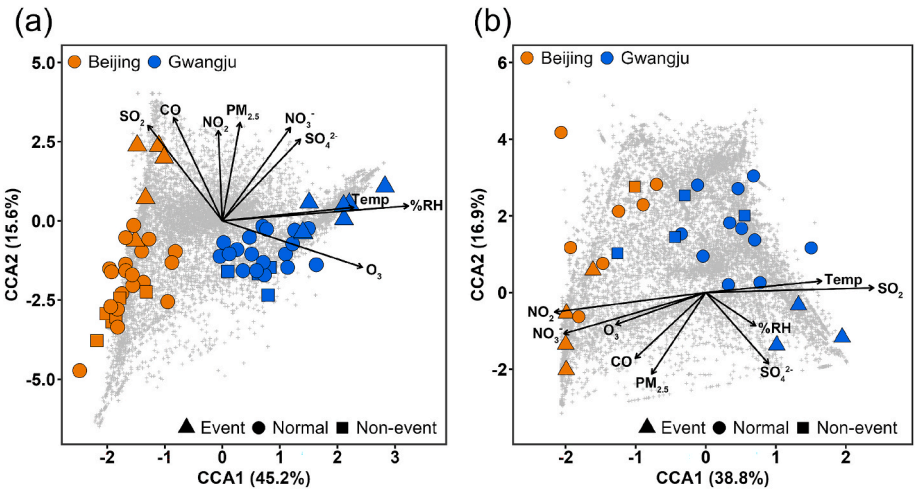


**Fig. 2.** Canonical correspondence analysis (CCA) score plots of WSOC profiles of $PM_{2.5}$ collected during winter (a) and summer (b) at the Beijing and Gwangju sites encompassing variables including inorganic gaseous species (including CO, $SO_2$, $NO_2$, $O_3$), particulate ions (including $NO_3^-$, $SO_4^{2-}$), and meteorological conditions (including Temp and %RH). Triangle, square and circle indicate haze event (daily mean $PM_{2.5}$ concentration of over 100 μg $m^{-3}$), normal (daily mean $PM_{2.5}$ concentration of over or equal to 30 μg $m^{-3}$ and less than or equal to 100 μg $m^{-3}$), nonevent (daily mean $PM_{2.5}$ concentration of less than 30 μg $m^{-3}$) days, respectively, and grey crosses represent the individual WSOC formulas.

WSOC collected in winter may reflect more local characteristics than those in summer. As the molecular composition of SOC comes from the transformation of POC (Hallquist et al., 2009; McNeill, 2015), the constituents of SOC are likely reflect the local primary sources. Although the van Krevelen plots and CCA results of WSOC-derived organic molecules showed seasonally and regionally different profiles of WSOC samples (see Figs. 1 and 2), it was insufficient to describe the SOC-related components in detail, so we further introduced other factors to discriminate the SOC-associated molecular features from the entire WSOC molecular species.

According to the air mass transport history analysis, each of three clusters of air masses occurred in Beijing and Gwangju sites, respectively, during the winter of 2019 (Fig. 3a and b). The fast-moving northwest air mass, passing through the inner Mongolia area (blue

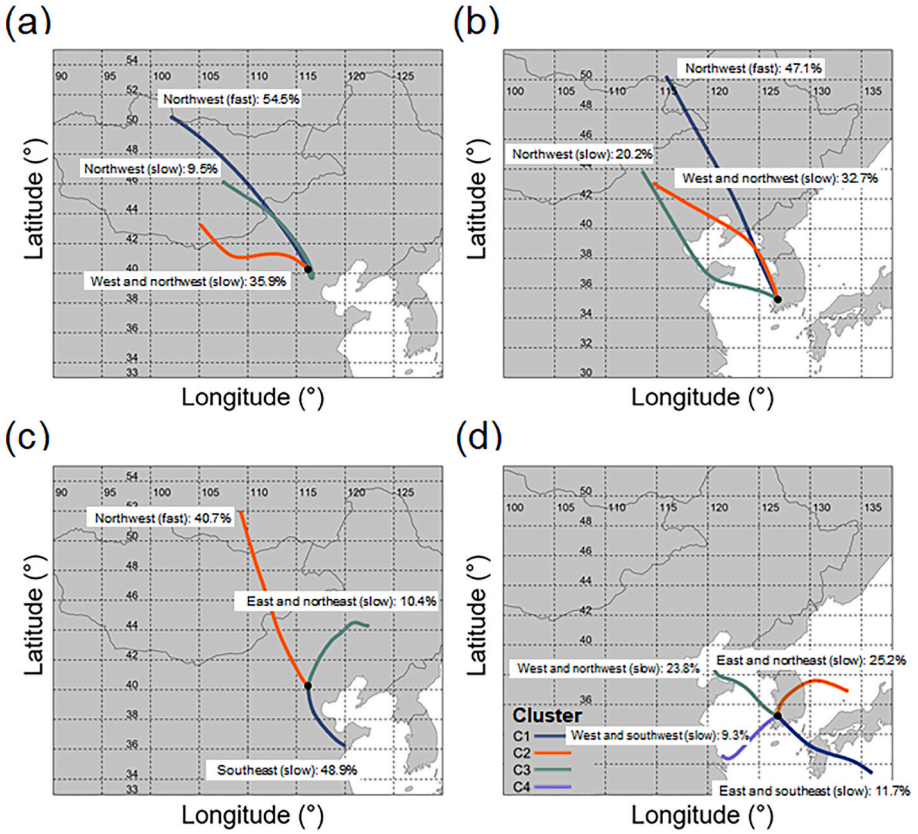


**Fig. 3.** Major clusters of air mass backward trajectories in (a) Beijing in Winter (2019), (b) Gwangju in Winter (2019), (c) Beijing in Summer (2019), and (d) Gwangju in Summer (2019) (72-h air mass backward trajectories arriving at the receptor site at the height of 100 m). The black dots indicate the locations of the sampling sites (the Beijing site, 40.14°N, 116.11°E; the Gwangju site, 35.13°N, 126.50°E).

line in Fig. 3a) dominated in the Beijing site, while Gwangju seemed more likely to be influenced with the fast-moving northwest air mass from the northeast China area (blue line in Fig. 3b). Conversely, the slow-moving west and northwest air masses (orange lines in Fig. 3a and b) were the most likely main driver during haze event in the Beijing site (the C2 cluster in Supplementary Fig. S4a), supporting that stagnant atmospheric conditions played a critical role in elevated $PM_{2.5}$ during the winter $PM_{2.5}$ (Park et al., 2020). It was also assumed that primary products under stagnant conditions could be the major precursors of winter SOC in Beijing, leading to more aromatic properties. During the winter period, the haze episodes occurred with the slow-moving west and northwest air masses (the C2 clusters in Supplementary Figs. S4a and b) and non-haze days are associated with the fast-moving northwest air masses (the C1 clusters in Supplementary Figs. S4a and b) in both sampling sites. The concentrations of $PM_{2.5}$ and WSOC significantly increased in the C2 cluster compared to the C1 cluster, but the chemical composition of WSOC (the proportions of CHO, CHON, CHOS, and CHONS species) did not change depending on the clusters, and increase in PCA was observed in the dominant C2 cluster in both regions during the winter (Supplementary Fig. S5).

During the summer of 2019, we observed three clusters of air masses in Beijing and four clusters of air masses in Gwangju (Fig. 3c and d). The slow-moving southwest air mass (48.9%, red line in Fig. 3c) was most prevalent in the Beijing site, followed by the fast-moving northwest air mass (40.7%) from the inner Mongolia area. Gwangju, in particular, was found to be more stagnant due to the influence of four different air masses in four different directions during the sampling period (Fig. 3d). Air mass cluster analysis showed that haze episodes in Beijing during summer were also significantly associated with WSOC, with decreased levels of CHO species and increased levels of CHOS species (Supplementary Fig. S5). Under the given meteorological conditions (higher % RH and Temp, and lower wind speeds), Gwangju was supposed to exhibit a more favorable environment for SOA formation process than Beijing during the Summer of 2019, resulting in the different chemical characteristics of SOC in the sampling sites, as shown in Fig. 4. Of course, other factors including gaseous species ($NO_2$, $SO_2$, and $O_3$) and particulate ions ($NO_3^-$ and $SO_4^{2-}$) can affect the composition of SOA. The gaseous and ion species data were obtained from our previous study (Oh et al., 2023; Park et al., 2020) and the overall environmental variables are summarized in Supplementary Dataset S0.

### 3.2. Determination of SOC-associated molecular features in WSOC compositions

According to the concentrations of SOC and POC estimated by using the WSOC-based method in this study, SOC accounted for 40.4% ± 6.2% of OCin Gwangju during the winter, while the contribution of SOC to OC decreased (18.1% ± 9.8%) in Beijing, supporting that the primary combustion products were a major contributor of air pollution in wintertime Beijing and the contribution of SOC in Gwangju was two times greater than that in Beijing. In addition, the SOC fraction in Gwangju contributed more (59.9% ± 10.1%) than that in Beijing

**Table 1**
Contributions of primary organic carbon (POC) and secondary organic carbon (SOC) in Beijing and Gwangju.

| Sampling site | Sampling season | WSOC (μg/m$^3$) | OC (μg/m$^3$) | Levoglucosan (μg/m$^3$) | POC (μg/m$^3$) [%] | SOC (μg/m$^3$) [%] |
|---|---|---|---|---|---|---|
| Beijing (China) | Winter | 2.0 ± 2.1 | 8.4 ± 5.9 | 0.096 ± 0.061 | 6.9 ± 4.7 [81.9 ± 9.8] | 1.8 ± 1.9 [18.1 ± 9.8] |
| | Summer | 2.1 ± 1.7 | 4.8 ± 1.8 | 0.026 ± 0.009 | 2.7 ± 0.8 [62.3 ± 20.1] | 2.1 ± 1.7 [37.7 ± 20.1] |
| Gwangju (Korea) | Winter | 2.9 ± 1.6 | 5.9 ± 3.1 | 0.157 ± 0.067 | 3.5 ± 1.8 [59.6 ± 6.2] | 2.4 ± 1.5 [40.4 ± 6.2] |
| | Summer | 2.4 ± 1.3 | 3.7 ± 1.9 | 0.027 ± 0.013 | 1.4 ± 0.7 [40.1 ± 10.1] | 2.3 ± 1.3 [59.9 ± 10.1] |

The daily WSOC, OC, and levoglucosan concentrations were obtained from our previous literatures (Oh et al., 2023; Park et al., 2020).

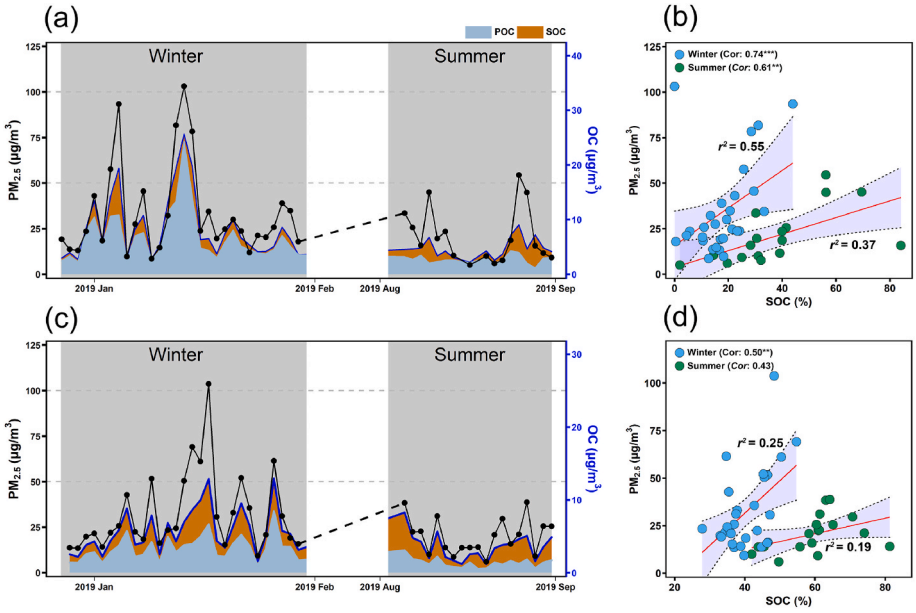


**Fig. 4.** Temporal distributions of measured $PM_{2.5}$ concentrations and POC & SOC concentrations estimated in this study at the Beijing (a) and Gwangju (c) sites during the study periods. Relationships between $PM_{2.5}$ and %SOC at Beijing (b) and Gwangju (d) sites. The colored dots in panels b and d denote the sampling seasons in each sampling site. Significance tests: $^{***}p < 0.001$, $^{**}p < 0.01$, $^{*}p < 0.05$.

(37.7% ± 20.1%) in the summer (Fig. 4). The mean concentrations and relative contributions of POC and SOC were summarized in Table 1 and Supplementary Tables S1 and 3.

The positive relationships between the mass of $PM_{2.5}$ and the relative fraction of SOC (%SOC) in OC at both sampling sites, shown in Fig. 4b and d, were agreed well with the report that the mass of secondary pollutants including SOA and secondary inorganic ions increased with increasing $PM_{2.5}$ mass (i.e., under more polluted atmospheric conditions) (Tong et al., 2016). The higher correlations of %SOC with $PM_{2.5}$ mass at the Beijing site than those at the Gwangju site were hypothesized by that the SOA formation can be more significantly influenced by primary precursor molecules in the atmosphere in Beijing (Fig. 4b), but the SOA formation in Gwangju were less significantly affected by the $PM_{2.5}$ mass (Fig. 4d), thus resulting in less $PM_{2.5}$ dependent trend in %SOC.

We also investigated their relationships of daily SOC concentrations with chemical and molecular classes of WSOC compositions (see Supplementary Fig. S6). Significant positive relationships with %CHONS and %Aliphatic and negative relationships with %CHO, %HUP and %PP were observed in Gwangju during winter, while no significant correlation was observed in Beijing. During the summer of 2019, no significant relationship of SOC concentrations with chemical and molecular classes was observed at both sites.

Furthermore, daily SOC concentrations at both sampling sites, estimated using the WSOC method above, were used to extract the SOC constituents from the FT-ICR MS-derived datasets. Spearman correlation analysis between daily SOC concentrations and the intensities of the assigned molecular formulas was applied to determine the SOC-associated molecular features from the FT-ICR MS-derived WSOC datasets. Van Krevelen diagrams were used to further elucidate the Spearman rank correlations between molecular formulas and indices of biomass burning and SOC. As shown in Fig. 5a and c, the SOC-associated molecular features were distinctly assigned during winter in both Beijing and Gwangju.

The majority of SOC in Beijing during winter was dominated by Aliphatics (42.2%), followed by HUP (37.2 %), PP (11.5%), PCA (3.0%) and others (6.1%), while at the Gwangju site Aliphatics (74.4%) and HUP (10.6%) accounted for 85.0%, and PCA, PP, and the remainders accounted for 8.0%, 1.1% and 5.9%, respectively (Supplementary Fig. S7). Comparatively, the majority of SOC in Beijing during summer was Aliphatics (45.4%) and HUP (28.4%), followed by PCA (10.4%), PP (1.8%), and others (14.8%), while at the Gwangju site the Aliphatics (62.7%), followed by HUP (30.9%), PCA (3.0%), PP (1.8%) and others (1.7%) were dominated, respectively (Supplementary Fig. S7).

### 3.3. *In-depth characterization of SOC-associated molecular features*

The mean ratio of mass to charge (m/z) was higher for the SOC-associated compositions (m/z ≈ 458.1 and 470.8, respectively) compared with the total WSOC formulae in both Beijing and Gwangju during wintertime (m/z ≈ 421.1 and 440.6, respectively) (Fig. 6). The higher mean m/z of SOC-molecular features during winter were supposed that the SOA formation products during winter mainly come from the oligomerization of the primary VOC precursors (i.e., glyoxal or α-pinene), resulting in higher molecular weight compounds compared to WSOC compositions (Tolocka et al., 2004; Trump and Donahue, 2014).

The relative contributions of CHO species in SOC fractions at the Beijing site (9.7% ± 1.9% for winter and 13.6% ± 6.2% for summer) were smaller than those at the Gwangju site (13.1% ± 5.5% for winter and 17.2% ± 6.4% for summer) regardless of the sampling seasons (see Supplementary Table S1). In particular, the CHO compounds showed broader O number distributions ($O_3$~$O_{19}$) during the summer than those during winter at both sampling sites (Supplementary Fig. S8), implying more oxidations of the CHO species during summer season, and it was agreed well with the higher O/C ratios of the assigned formulas in the summer season (see Supporting Datasets).

As the CHOS species was the most abundant in the WSOC at the Beijing site during winter, the CHOS fractions in SOC at the Beijing site during winter were 40.9% ± 3.9% of the total, while those in SOC

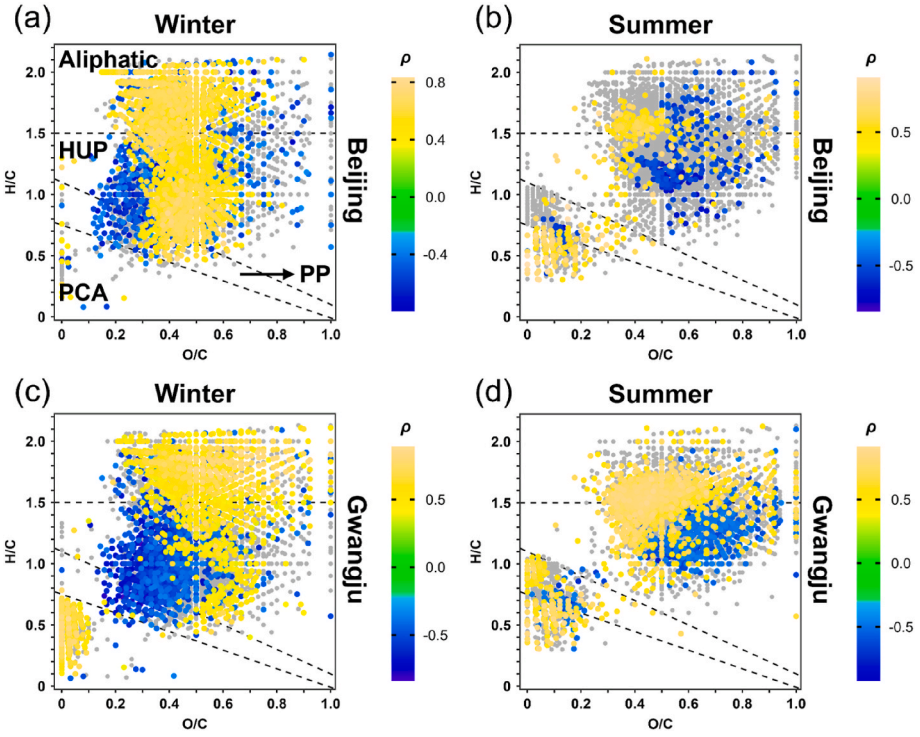


**Fig. 5.** Van Krevelen plots displaying the Spearman rank correlations (Spearman's rho, ρ) between SOC and the chemical formulas of $PM_{2.5}$-derived WSOC in this study. Only formulas with only $|r| > 0.4$ and $p < 0.05$ were presented in the van Krevelen diagram to simplify the plot. The compositions showing no significant correlation ($p > 0.05$) with SOC were colored grey. Compound classes include polycyclic condensed aromatics (PCA; $AI_{mod} > 0.66$), polyphenolic (PP; $0.5 < AI_{mod} \leq 0.66$), highly unsaturated and phenolic (HUP; $AI_{mod} \leq 0.5$ and $H/C < 1.5$), aliphatics ($1.5 \leq H/C < 2$).

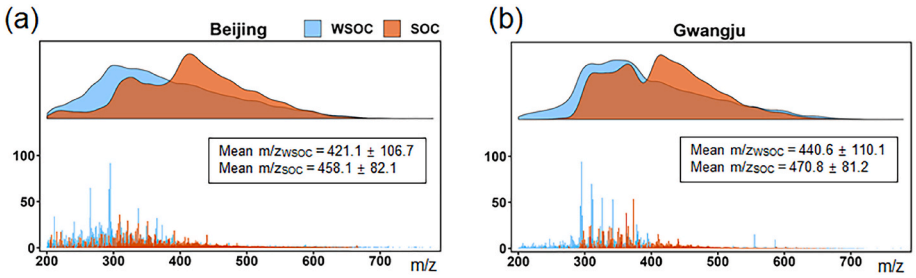


**Fig. 6.** Reconstructed mass spectra showing differences in molecular composition of WSOC and SOC-associated compounds at the (a) Beijing and (b) Gwangju sites in wintertime. The inserts included mean m/z values for WSOC and SOC spectral profiles, respectively. The upper panel represents a rendered profile of the corresponding spectrum.

accounted for 44.2% ± 11.5% during summer (Supplementary Table S1). At the Gwangju site, the CHOS species in SOC were 28.5% ± 3.5% and 33.6% ± 5.4% for winter and summer, respectively. It was assumed that the CHOS class species are the major products of SOC at both Beijing and Gwangju sites, and the contribution of CHOS species was more dominant at Beijing than one at Gwangju. Among the sulfur-containing molecules, the formulas with O/S ≥ 4 were considered as organosulfate species, as demonstrated previously (Tong et al., 2016). The CHOS compounds contain one or two sulfur atoms and more than 99.8% ± 0.1% (for Beijing) or 99.7% ± 0.2% (for Gwangju) of them during winter and 97.2% ± 2.3% (for Beijing) or 98.5% ± 1.2% (for Gwangju) of them during summer exhibit O/S ratios greater than 4 (Supplementary Table S4), implying the CHOS species in SOC fractions exist as a form of organosulfate.

The CHON proportions in the SOC at the Beijing site during winter were 29.7% ± 4.2% of the total, and the corresponding fraction during summer was 25.7% ± 6.8%. At Gwangju site, the CHON species in SOC accounted for 19.5% ± 4.7% for winter and 33.3% ± 8.1% for summer (Supplementary Table S1). Thus, it seems that the CHON class species are one of the major products of SOC at both Beijing and Gwangju during the winter and summer. As the presence of organonitrate compounds from the CHON class species can be estimated with the formulas with O/N ≥ 3 (Ning et al., 2022), the organonitrates were found to be present in SOC-associated CHON species with about 80% of the total throughout the sampling seasons at the Beijing site (Supplementary Table S4). In comparison, organonitrates accounted for 73.5% ± 14.1% of the total SOC species for winter and increased up to 94.9% ± 1.4% for summer at the Gwangju site, showing the increased contribution of organonitrate on the SOC composition in Gwangju during summer. Taken together, the relative contributions of organonitrate as one of the constituents of CHON in SOA were not changed in Beijing during Winter and Summer of 2019, but in Gwangju the organonitrate was more dominant during summer. The remaining fractions of SOC-associated CHON class compounds might exist as a form of nitriles, amides, amines, and nitro compounds (Booyens et al., 2019; Malloy et al., 2009).

CHONS species occupied 19.4% ± 4.0% and 15.7% ± 6.9% of the total SOC at the Beijing site during winter and summer, respectively, while it accounted for 35.8% ± 8.5% and 15.5% ± 3.1% for winter and summer at the Gwangju site (Supplementary Table S1). Among the sulfur and nitrogen-containing molecules, the formulas with O/(4S+3N) ≥1 were considered as organosulfate and/or nitrooxy organosulfates species. In Beijing 93.1% ± 3.5% of CHONS species during winter and 83.9% ± 10.8% during summer were. 99.2% ± 0.3% for winter and 88.4% ± 5.8% for summer at Gwangju (Supplementary Table S4). Higher proportions of oxidized organosulfates and/or nitrooxy organosulfates (~99.7%) in SOC during winter compared to those (~86.1%) during summer perhaps indicate the presence of stronger drivers to the formations of oxidized organosulfates or nitrooxy organosulfates. Our observations that more than 80% by number of the assigned CHONS species largely exhibit oxidized organosulfates and/or nitrooxy organosulfates were agreed well with the previous report by Jiang et al. (2022).

## 4. Conclusions

We conducted a comparative analysis of SOA-associated molecular features in $PM_{2.5}$ collected at different regions (Beijing in China and Gwangju in Korea) during different seasons (winter and summer). WSOC fractions of the $PM_{2.5}$ samples were analyzed using FT-ICR MS to obtain detailed chemical compositions of the $PM_{2.5}$-derived WSOC samples. The SOC-associated fraction was then discriminated from the fraction of biomass burning in the FT-ICR MS-derived WSOC datasets using the $WSOC_{BB}$ and $WSOC_{NBB}$ indices.

Correlations of %SOC with $PM_{2.5}$ mass in Fig. 4 showed that SOA formation in Beijing was more influenced by primary emission sources than in Gwangju. Following molecular characterization of SOC fractions revealed that the SOC fractions in Gwangju exhibit more aliphatic natures and those in Beijing were more likely highly unsaturated and phenolic compounds (HUP), showing their different precursors and formation processes. Higher %RH and Temp, and stagnant atmospheric condition (lower wind speeds) in Gwangju during summer was the most significant driver to SOA formation, thereby resulting in more aliphatic nature of SOC, compared to those in Beijing.

The WSOC-based SOC estimation method used in this study might have certain uncertainty perhaps due to the inaccuracy of the estimated SOC fraction. The measured levoglucosan to OC ratio can vary by sampling regions and seasons, it will also be different depending on combustion condition and type of biomass burned. $PM_{2.5}$-derived SOC fractions exhibit a very complex composition consisting of organic molecules containing a wide range of functional groups including carboxylic acid and carbonyl but also oxidized and reduced nitrogen and/or sulfur groups, and those highly variable organic compositional characteristics and concentrations can be significantly influenced by environmental and meteorological conditions (i.e., gaseous species, particulate ions, temperature and relative humidity). Additionally, the criteria used in this study (i.e., O/S ≥ 4, O/N ≥ 3, or O/(4S+4N) ≥ 1) were not absolute conditions describing the presence of OS or ON, and there may be some discrepancies between the actual compositions. Nevertheless, it was worthwhile to use these criteria to compare the apparent profiles of SOC composition between different sites in different seasons. Therefore, it is noted that the detailed compositional characteristics of SOC fraction and the correlation with other environmental factors can be a key to understanding the complicated formation mechanism of SOA, and will be used as a control measure to solve the haze problem in Northeast Asia.

## CRediT authorship contribution statement

**Min Sung Kim:** Methodology, Software, Validation, Investigation, Visualization, Writing – original draft. **Yujue Wang:** Methodology, Formal analysis, Data curation, Writing – review & editing. **Mira Choi:** Methodology, Validation, Formal analysis, Data curation. **Shiyi Chen:**

Methodology, Validation, Investigation. **Min-Suk Bae:** Term, Methodology, Writing – review & editing. **Kihong Park:** Term, Methodology, Resources, Writing – review & editing. **Min Hu:** Term, Resources, Writing – review & editing, Supervision. **Kyoung-Soon Jang:** Conceptualization, Writing – original draft, Writing – review & editing, Supervision, Project administration, Funding acquisition.

## Declaration of competing interest

The authors declare that they have no known competing financial interests or personal relationships that could have appeared to influence the work reported in this paper.

## Data availability

Data will be made available on request.

## Acknowledgements

This research was supported by the National Strategic Project-Fine Particle of the National Research Foundation of Korea (NRF) funded by the Ministry of Science and ICT (MSIT), the Ministry of Environment, and the Ministry of Health and Welfare (NRF-2017M3D8A1092223), the FRIEND (Fine Particle Research Initiative in East Asia Considering National Differences) Project through the NRF funded by the MSIT (2020M3G1A1114551) and KBSI (C330222) grants.

## Appendix A. Supplementary data

Supplementary data to this article can be found online at https://doi.org/10.1016/j.atmosenv.2023.120235.

## References

Altieri, K.E., Seitzinger, S.P., Carlton, A.G., Turpin, B.J., Klein, G.C., Marshall, A.G., 2008. Oligomers formed through in-cloud methylglyoxal reactions: chemical composition, properties, and mechanisms investigated by ultra-high resolution FT-ICR mass spectrometry. Atmos. Environ. 42, 1476–1490.

Arimoto, R., Duce, R.A., Savoie, D.L., Prospero, J.M., Talbot, R., Cullen, J.D., Tomza, U., Lewis, N.F., Ray, B.J., 1996. Relationships among aerosol constituents from Asia and the north pacific during PEM-west A. J Geophys Res-Atmosphere 101, 2011–2023.

Arimoto, R., Zhang, X.Y., Huebert, B.J., Kang, C.H., Savoie, D.L., Prospero, J.M., Sage, S. K., Schloesslin, C.A., Khaing, H.M., Oh, S.N., 2004. Chemical composition of atmospheric aerosols from Zhenbeitai, China, and Gosan, South Korea, during ACE-Asia. J Geophys Res-Atmosphere 109, D19S04.

Babar, Z.B., Park, J.H., Kang, J., Lim, H.J., 2016. Characterization of a smog chamber for studying formation and physicochemical properties of secondary organic aerosol. Aerosol Air Qual. Res. 16, 3102–3113.

Bianco, A., Deguillaume, L., Chaumerliac, N., Vaïtilingom, M., Wang, M., Delort, A.M., Bridoux, M.C., 2019. Effect of endogenous microbiota on the molecular composition of cloud water: a study by Fourier-transform ion cyclotron resonance mass spectrometry (FT-ICR MS). Sci. Rep. 9, 7663.

Bogawski, P., Borycka, K., Grewling, L., Kasprzyk, I., 2019. Detecting distant sources of airborne pollen for Poland: integrating back-trajectory and dispersion modelling with a satellite-based phenology. Sci. Total Environ. 689, 109–125.

Bond, T.C., Doherty, S.J., Fahey, D.W., Forster, P.M., Berntsen, T., DeAngelo, B.J., Flanner, M.G., Ghan, S., Kärcher, B., Koch, D., Kinne, S., Kondo, Y., Quinn, P.K., Sarofim, M.C., Schultz, M.G., Schulz, M., Venkataraman, C., Zhang, H., Zhang, S., Bellouin, N., Guttikunda, S.K., Hopke, P.K., Jacobson, M.Z., Kaiser, J.W., Klimont, Z., Lohmann, U., Schwarz, J.P., Shindell, D., Storelvmo, T., Warren, S.G., Zender, C.S., 2013. Bounding the role of black carbon in the climate system: a scientific assessment. J. Geophys. Res. Atmos. 118, 5380–5552.

Booyens, W., Van Zyl, P.G., Peukes, J.P., Ruiz-Jimenez, J., Kopperi, M., Riekkola, M.L., Vakkari, V., Josipovic, M., Kulmala, M., Laakso, L., 2019. Characterising particulate organic nitrogen at A savannah-grassland region in South Africa. Atmosphere 10, 492.

Calvo, A.I., Martins, V., Nunes, T., Duarte, M., Hillamo, R., Teinila, K., Pont, V., Castro, A., Fraile, R., Tarelho, L., Alves, C., 2015. Residential wood combustion in two domestic devices: relationship of different parameters throughout the combustion cycle. Atmos. Environ. 116, 72–82.

Carslaw, D.C., Ropkins, K., 2012. Openair — an R package for air quality data analysis. Environ. Model. Software 27–28, 52–61.

Choi, J., Park, R.J., Lee, H.M., Lee, S., Jo, D.S., Jeong, J.I., Henze, D.K., Woo, J.H., Ban, S. J., Lee, M.D., Lim, C.S., Park, M.K., Shin, H.J., Cho, S., Peterson, D., Song, C.K., 2019a. Impacts of local vs. trans-boundary emissions from different sectors on PM2.5 exposure in South Korea during the KORUS-AQ campaign. Atmos. Environ. 203, 196–205.

Choi, J.H., Jang, E., Yoon, Y.J., Park, J.Y., Kim, T.W., Becagli, S., Caiazzo, L., Cappelletti, D., Krejci, R., Eleftheriadis, K., Park, K.T., Jang, K.S., 2019b. Influence of biogenic organics on the chemical composition of Arctic aerosols. Global Biogeochem. Cycles 33, 1238–1250.

Chuang, W.K., Donahue, N.M., 2017. Dynamic consideration of smog chamber experiments. Atmos. Chem. Phys. 17, 10019–10036.

Chung, S.H., Seinfeld, J.H., 2002. Global distribution and climate forcing of carbonaceous aerosols. J. Geophys. Res. 107, 4407–4440.

Coward, E.K., Ohno, T., Sparks, D.L., 2019. Direct evidence for temporal molecular fractionation of dissolved organic matter at the iron oxyhydroxide interface. Environ. Sci. Technol. 53, 642–650.

Crawford, J.H., Ahn, J.Y., Al-Saadi, J., Chang, L., Emmons, L.K., Kim, J., Lee, G., Park, J. H., Park, R.J., Woo, J.H., Song, C.K., Hong, J.H., Hong, Y.D., Lefer, B.L., Lee, M., Lee, T., Kim, S., Min, K.E., Yum, S.S., Shin, H.J., Kim, Y.W., Choi, J.S., Park, J.S., Szykman, J.J., Long, R.W., Jordan, C.E., Simpson, I.J., Fried, A., Dibb, J.E., Cho, S., Kim, Y.P., 2021. The Korea-United States air quality (KORUS-AQ) field study. Elementa 12, 1–27.

Decesari, S., Fuzzi, S., Facchini, M.C., Mircea, M., Emblico, L., Cavalli, F., Maenhaut, W., Chi, X., Schkolnik, G., Falkovich, A., Rudich, Y., Claeys, M., Pashynska, V., Vas, G., Kourtchev, I., Vermeylen, R., Hoffer, A., Andreae, M.O., Tagliavini, E., Moretti, F., Artaxo, P., 2006. Characterization of the organic composition of aerosols from Rondônia, Brazil, during the LBA-SMOCC 2002 experiment and its representation through model compounds. Atmos. Chem. Phys. 6, 375–402.

Draxler, R.R., Hess, G.D., 1998. An overview of the HYSPLIT_4 modelling system for trajectories, dispersion, and deposition. Aust. Meteorol. Mag. 47, 295–308.

Feng, J., Li, M., Zhang, P., Gong, S., Zhong, M., Wu, M., Zheng, M., Chen, C., Wang, H., Lou, S., 2013. Investigation of the sources and seasonal variations of secondary organic aerosols in PM2.5 in Shanghai with organic tracers. Atmos. Environ. 79, 614–622.

Fine, P.M., Cass, G.R., Simoneit, B.R., 2001. Chemical characterization of fine particle emissions from fireplace combustion of woods grown in the northeastern United States. Environ. Sci. Technol. 35, 2665–2675.

Gonçalves, C., Alves, C., Fernandes, A.P., Monteiro, C., Tarelho, L., Evtyugina, M., Pio, C., 2011. Organic compounds in PM2.5 emitted from fireplace and woodstove combustion of typical Portuguese wood species. Atmos. Environ. 45, 4533–4545.

Guo, X., Zhao, L., Chen, D., Jia, Y., Zhao, N., Liu, W., Cheng, S., 2018. Air quality improvement and health benefit of PM(2.5) reduction from the coal cap policy in the Beijing-Tianjin-Hebei (BTH) region, China. Environ. Sci. Pollut. Res. Int. 25, 32709–32720.

Halliday, H.S., DiGangi, J.P., Choi, Y., Diskin, G.S., Pusede, S.E., Rana, M., Nowak, J.B., Knote, C., Ren, X., He, H., Dickerson, R.R., Li, Z., 2019. Using short-term CO/CO2 ratios to assess air mass differences over the Korean peninsula during KORUS-AQ. J Geophys Res-Atmosphere 124, 20.

Hallquist, M., Wenger, J.C., Baltensperger, U., Rudich, Y., Simpson, D., Claeys, M., Dommen, J., Donahue, N.M., George, C., Goldstein, A.H., Hamilton, J.F., Herrmann, H., Hoffmann, T., Iinuma, Y., Jang, M., Jenkin, M.E., Jimenez, J.L., Kiendler-Scharr, A., Maenhaut, W., McFiggans, G., Mentel, T.F., Monod, A., Prévôt, A.S.H., Seinfeld, J.H., Surratt, J.D., Szmigielski, R., Wildt, J., 2009. The formation, properties and impact of secondary organic aerosol: current and emerging issues. Atmos. Chem. Phys. 9, 5155–5236.

Han, D., Wang, Z., Cheng, J., Wang, Q., Chen, X., Wang, H., 2017. Volatile organic compounds (VOCs) during non-haze and haze days in Shanghai: characterization and secondary organic aerosol (SOA) formation. Environ. Sci. Pollut. Res. Int. 24, 18619–18629.

Heintzenberg, J., 1989. Fine particles in the global troposphere A review. Tellus B 41, 149–160.

Hoell, J.M., Davis, D.D., Liu, S.C., Newell, R., Shipham, M., Akimoto, H., McNeal, R.J., Bendura, R.J., Drewry, J.W., 1996. Pacific exploratory mission-west A (PEM-west A): september–october 1991. J Geophys Res-Atmosphere 101, D1.

Hoffmann, T., Odum, J.R., Bowman, F., Collins, D., Klockow, D., Flagan, R.C., Seinfeld, J. H., 1997. Formation of organic aerosols from the oxidation of biogenic hydrocarbons. J. Atmos. Chem. 26, 189–222.

Huang, R.J., Zhang, Y., Bozzetti, C., Ho, K.F., Cao, J.J., Han, Y., Daellenbach, K.R., Slowik, J.G., Platt, S.M., Canonaco, F., Zotter, P., Wolf, R., Pieber, S.M., Bruns, E.A., Crippa, M., Ciarelli, G., Piazzalunga, A., Schwikowski, M., Abbaszade, G., Schnelle-Kreis, J., Zimmermann, R., An, Z., Szidat, S., Baltensperger, U., El Haddad, I., Prevot, A.S., 2014. High secondary aerosol contribution to particulate pollution during haze events in China. Nature 514, 218–222.

Jang, K.S., Choi, A.Y., Choi, M., Kang, H., Kim, T.W., Park, K.T., 2019. Size-segregated chemical compositions of HULISs in ambient aerosols collected during the winter season in songdo, South Korea. Atmosphere 10, 226.

Jang, K.S., Choi, M., Park, M., Park, M.H., Kim, Y.H., Seo, J., Wang, Y., Hu, M., Bae, M.S., Park, K., 2020. Assessment of PM(2.5)-bound nitrogen-containing organic compounds (NOCs) during winter at urban sites in China and Korea. Environ. Pollut. 265, 114870.

Jiang, H., Li, J., Tang, J., Cui, M., Zhao, S., Mo, Y., Tian, C., Zhang, X., Jiang, B., Liao, Y., Chen, Y., Zhang, G., 2022. Molecular characteristics of organosulfur compounds in guangzhou, South China: heterogeneous secondary reactions drivers the molecular distribution. Atmos. Chem. Phys. 22, 6919–6935.

Jimenez, J.L., Jayne, J.T., Shi, Q., Kolb, C.E., Worsnop, D.R., Yourshaw, I., Seinfeld, J.H., Flagan, R.C., Zhang, X., Smith, K.A., Morris, J.W., Davidovits, P., 2003. Ambient aerosol sampling using the aerodyne aerosol mass spectrometer. J. Geophys. Res. 108, 8425.

Jin, Y., Yan, C., Sullivan, A.P., Liu, Y., Wang, X., Dong, H., Chen, S., Zeng, L., Collett, J.L., Zheng, M., 2020. Significant contribution of primary sources to water-soluble organic carbon during spring in Beijing, China. Atmosphere 11, 395.
Jing, B., Tong, S., Liu, Q., Li, K., Wang, W., Zhang, Y., Ge, M., 2016. Hygroscopic behavior of multicomponent organic aerosols and their internal mixtures with ammonium sulfate. Atmos. Chem. Phys. 16, 4101–4118.
Jorga, S.D., Kaltsonoudis, C., Liangou, A., Pandis, S.N., 2020. Measurement of formation rates of secondary aerosol in the ambient urban atmosphere using a dual smog chamber system. Environ. Sci. Technol. 54, 1336–1343.
Kasper-Giebl, A., Kaling, M.F., Puxbaum, H., 1999. Scavenging ratios for sulfate, ammonium and nitrate determined at Mt. Sonnblick (3106 m a.s.l.). Atmos. Environ. 33, 895–906.
Kim, S., Kramer, R.W., Hatcher, P.G., 2003. Graphical method for analysis of ultrahigh-resolution broadband mass spectra of natural organic matter, the van Krevelen diagram. Anal. Chem. 75, 5336–5344.
Koch, B.P., Dittmar, T., 2006. From mass to structure: an aromaticity index for high-resolution mass data of natural organic matter. Rapid Commun. Mass Spectrom. 20, 926–932.
Koch, B.P., Dittmar, T., 2016. From mass to structure: an aromaticity index for high-resolution mass data of natural organic matter. Rapid Commun. Mass Spectrom. 30, 250.
Kondo, Y., Miyazaki, Y., Takegawa, N., Miyakawa, T., Weber, R.J., Jimenez, J.L., Zhang, Q., Worsnop, D.R., 2007. Oxygenated and water-soluble organic aerosols in Tokyo. J. Geophys. Res. Atmos. 112, D01203.
Kroll, J.H., Seinfeld, J.H., 2008. Chemistry of secondary organic aerosol: formation and evolution of low-volatility organics in the atmosphere. Atmos. Environ. 42, 3593–3624.
Ksionzek, K.B., Lechtenfeld, O.J., McCallister, S.L., Schmitt-Kopplin, P., Geuer, J.K., Geibert, W., Koch, B.P., 2016. Dissolved organic sulfur in the ocean: biogeochemistry of a petagram inventory. Science 354, 456–459.
Lee, K.Y., Batmunkh, T., Joo, H.S., Park, K., 2018. Comparison of the physical and chemical characteristics of fine road dust at different urban sites. J. Air Waste Manag. Assoc. 68, 812–823.
Li, J., Han, Z., Li, J., Liu, R., Wu, Y., Liang, L., Zhang, R., 2020. The formation and evolution of secondary organic aerosol during haze events in Beijing in wintertime. Sci. Total Environ. 703, 134937.
Liu, T., Wang, X., Deng, W., Hu, Q., Ding, X., Zhang, Y., He, Q., Zhang, Z., Lü, S., Bi, X., Chen, J., Yu, J., 2015. Secondary organic aerosol formation from photochemical aging of light-duty gasoline vehicle exhausts in a smog chamber. Atmos. Chem. Phys. 15, 9049–9062.
Liu, L., Zhang, L., Wen, W., Jiao, J., Cheng, H., Ma, X., Sun, C., 2023. Chemical composition, oxidative potential and identifying the sources of outdoor PM(2.5) after the improvement of air quality in Beijing. Environ. Geochem. Health 45, 1537–1553.
Malloy, Q.G.J., Qi, L., Warren, B., Cocker III, D.R., Erupe, M.E., Silva, P.J., 2009. Secondary organic aerosol formation from primary aliphatic amines with NO3 radical. Atmos. Chem. Phys. 9, 2051–2060.
Matsumoto, K., 2022. Atmospheric deposition fluxes and processes of the water-soluble and water-insoluble organic carbon in central Japan. Atmos. Environ. 271, 118913.
Mayorga, R.J., Zhao, Z., Zhang, H., 2021. Formation of secondary organic aerosol from nitrate radical oxidation of phenolic VOCs: implications for nitration mechanisms and brown carbon formation. Atmos. Environ. 244, 117910.
McNeill, V.F., 2015. Aqueous organic chemistry in the atmosphere: sources and chemical processing of organic aerosols. Environ. Sci. Technol. 49, 1237–1244.
Ning, C., Gao, Y., Zhang, H., Wang, L., Yu, H., Zou, L., Cao, R., Chen, J., 2022. Molecular chemodiversity of water-soluble organic matter in atmospheric particulate matter and their associations with atmospheric conditions. Sci. Total Environ. 809, 151171.
Oh, S.H., Park, E.H., Yi, S.M., Shon, Z.H., Park, K., Bae, M.S., 2018. Contribution of biomass burning and secondary organic carbon to water soluble organic carbon at a suburban site. J Korean Soc Atmos Environ 34, 259–268.
Oh, S.H., Park, K., Park, M., Song, M., Jang, K.S., Schauer, J.J., Bae, G.N., Bae, M.S., 2023. Comparison of the sources and oxidative potential of PM(2.5) during winter time in large cities in China and South Korea. Sci. Total Environ. 859, 160369.
Oksanen, J., Blanchet, F.G., Kindt, R., Legendre, P., Minchin, P.R., O'Hara, R.B., Simpson, G.L., Solymos, P., Stevens, M.H.H., Wagner, H., 2014. Vegan: Community Ecology Package. R Package Version 2.2-0.
Olcese, L.E., Penner, J.E., Sillman, S., 2007. Development of a secondary organic aerosol formation mechanism: comparison with smog chamber experiments and atmospheric measurements. Atmos. Chem. Phys. Discuss. 7, 8361–8393.
Park, M., Wang, Y., Chong, J., Lee, H., Jang, J., Song, H., Kwak, N., Borlaza, L.J.S., Maeng, H., Cosep, E.M.R., Denna, M.C.F.J., Chen, S., Seo, I., Bae, M.S., Jang, K.S., Choi, M., Kim, Y.H., Park, M., Ryu, J.S., Park, S., Hu, M., Park, K., 2020. Simultaneous measurements of chemical compositions of fine particles during winter haze period in urban sites in China and Korea. Atmosphere 11, 292.
Park, R.J., Oak, Y.J., Emmons, L.K., Kim, C.H., Pfister, G.G., Carmichael, G.R., Saide, P. E., Cho, S.Y., Kim, S., Woo, J.H., Crawford, J.H., Gaubert, B., Lee, H.J., Park, S.Y., Jo, Y.J., Gao, M., Tang, B., Stanier, C.O., Shin, S.S., Park, H.Y., Bae, C., Kim, E., 2021. Multi-model intercomparisons of air quality simulations for the KORUS-AQ campaign. Elementa 9, 00139.
Peterson, D.A., Hyer, E.J., Han, S.O., Crawford, J.H., Park, R.J., Holz, R., Kuehn, R.E., Eloranta, E., Knote, C., Jordan, C.E., Lefer, B.L., 2019. Meteorology influencing springtime air quality, pollution transport, and visibility in Korea. Elementa 7, 57.
Poschl, U., 2005. Atmospheric aerosols: composition, transformation, climate and health effects. Angew Chem. Int. Ed. Engl. 44, 7520–7540.
Puxbaum, H., Caseiro, A., Sanchez-Ochoa, A., Kasper-Giebl, A., Claeys, M., Gelencser, A., Legrand, M., Preunkert, S., Pio, C., 2007. Levoglucosan levels at background sites in Europe for assessing the impact of biomass combustion on the European aerosol background. J. Geophys. Res. 112, D23S05.
Qi, X., Zhu, S., Zhu, C., Hu, J., Lou, S., Xu, L., Dong, J., Cheng, P., 2020. Smog chamber study of the effects of NOx and NH3 on the formation of secondary organic aerosols and optical properties from photo-oxidation of toluene. Sci. Total Environ. 727, 138632.
R Core Team, 2020. R: A Language and Environment for Statistical Computing. R Foundation for Statistical Computing, Vienna, Austria. https://www.R-project.org/.
Reinhardt, A., Emmenegger, C., Gerrits, B., Panse, C., Dommen, J., Baltensperger, U., Zenobi, R., Kalberer, M., 2007. Ultrahigh mass resolution and accurate mass measurements as a tool to characterize oligomers in secondary organic aerosols. Anal. Chem. 79, 4074–4082.
Salma, I., Németh, Z., Weidinger, T., Maenhaut, W., Claeys, M., Molnár, M., Major, I., Ajtai, T., Utry, N., Bozóki, Z., 2017. Source apportionment of carbonaceous chemical species to fossil fuel combustion, biomass burning and biogenic emissions by a coupled radiocarbon–levoglucosan marker method. Atmos. Chem. Phys. 17, 13767–13781.
Sannigrahi, P., Sullivan, A.P., Weber, R.J., Ingall, E.D., 2006. Characterization of water-soluble organic carbon in urban atmospheric aerosols using solid-state 13C NMR spectroscopy. Environ. Sci. Technol. 40, 666–672.
Saxena, P., Hildemann, L.M., 1996. Water-soluble organics in atmospheric particles: a critical review of the literature and application of thermodynamics to identify candidate compounds. J. Atmos. Chem. 24, 57–109.
Seinfeld, J.H., Pandis, S.N., 2016. Atmospheric Chemistry and Physics: from Air Pollution to Climate Change. John Wiley & Sons Inc., New York, NY, USA.
Seinfeld, J.H., Pankow, J.F., 2003. Organic atmospheric particulate material. Annu. Rev. Phys. Chem. 54, 121–140.
Sirois, A., Bottenheim, J.W., 1995. Use of backward trajectories to interpret the 5-year record of PAN and O3 ambient air concentrations at Kejimkujik National Park, Nova Scotia. J. Geophys. Res. Atmos. 100, 2867–2881.
Song, M., Kim, M., Oh, S.H., Park, C., Kim, M., Kim, M., Lee, H., Choe, S., Bae, M.S., 2021. Influences of organic volatile compounds on the secondary organic carbon of fine particulate matter in the fruit tree area. Appl. Sci. 11, 8193.
terBraak, C.J.F., Verdonschot, P.F.M., 1995. Canonical correspondence analysis and related multivariate methods in aquatic ecology. Aquat. Sci. 57, 255–289.
Tolocka, M.P., Jang, M., Ginter, J.M., Cox, F.J., Kamens, R.M., Johnston, M.V., 2004. Formation of oligomers in secondary organic aerosol. Environ. Sci. Technol. 38, 1428–1434.
Tong, H., Kourtchev, I., Pant, P., Keyte, I.J., O'Connor, I.P., Wenger, J.C., Pope, F.D., Harrison, R.M., Kalberer, M., 2016. Molecular composition of organic aerosols at urban background and road tunnel sites using ultra-high resolution mass spectrometry. Faraday Discuss 189, 51–68.
Topping, D., Coe, H., McFiggans, G., Burgess, R., Allan, J., Alfarra, M.R., Bower, K., Choularton, T.W., Decesari, S., Facchini, M.C., 2004. Aerosol chemical characteristics from sampling conducted on the island of jeju, Korea during ACE Asia. Atmos. Environ. 38, 2111–2123.
Trump, E.R., Donahue, N.M., 2014. Oligomer formation within secondary organic aerosols: equilibrium and dynamic considerations. Atmos. Chem. Phys. 14, 3691–3701.
Tsigaridis, K., Kanakidou, M., 2003. Global modelling of secondary organic aerosol in the troposphere: a sensitivity analysis. Atmos. Chem. Phys. 3, 1849–1869.
Turpin, B.J., Saxena, P., Andrews, E., 2000. Measuring and simulating particulate organics in the atmosphere: problems and prospects. Atmos. Environ. 34, 2983–3013.
Wang, J., Ye, J., Zhang, Q., Zhao, J., Wu, Y., Li, J., Liu, D., Li, W., Zhang, Y., Wu, C., Xie, C., Qin, Y., Lei, Y., Huang, X., Guo, J., Liu, P., Fu, P., Li, Y., Lee, H.C., Choi, H., Zhang, J., Liao, H., Chen, M., Sun, Y., Ge, X., Martin, S.T., Jacob, D.J., 2021. Aqueous production of secondary organic aerosol from fossil-fuel emissions in winter Beijing haze. Proc. Natl. Acad. Sci. U.S.A. 118.
Wang, J., Gao, A., Li, S., Liu, Y., Zhao, W., Wang, P., Zhang, H., 2023. Regional joint PM (2.5)-O(3) control policy benefits further air quality improvement and human health protection in Beijing-Tianjin-Hebei and its surrounding areas. J. Environ. Sci. (China) 130, 75–84.
Weber, R.J., Sullivan, A.P., Peltier, R.E., Russell, A., Yan, B., Zheng, M., de Gouw, J., Warneke, C., Brock, C., Holloway, J.S., Atlas, E.L., Edgerton, E., 2007. A study of secondary organic aerosol formation in the anthropogenic-influenced southeastern United States. J. Geophys. Res. 112, D13302.
Wozniak, A.S., Bauer, J.E., Sleighter, R.L., Dickhut, R.M., Hatcher, P.G., 2008. Technical Note: molecular characterization of aerosol-derived water soluble organic carbon using ultrahigh resolution electrospray ionization Fourier transform ion cyclotron resonance mass spectrometry. Atmos. Chem. Phys. 8, 5099–5111.
Yang, X., Liu, S., Shao, P., He, J., Liang, Y., Zhang, B., Liu, B., Liu, Y., Tang, G., Ji, D., 2020. Effectively controlling hazardous airborne elements: insights from continuous hourly observations during the seasons with the most unfavorable meteorological conditions after the implementation of the APPCAP. J. Hazard Mater. 387, 121710.
Zhang, Y., Li, X., Nie, T., Qi, J., Chen, J., Wu, Q., 2018. Source apportionment of PM2.5 pollution in the central six districts of Beijing, China. J. Clean. Prod. 174, 661–669.
Zheng, Y., Chen, Q., Cheng, X., Mohr, C., Cai, J., Huang, W., Shrivastava, M., Ye, P., Fu, P., Shi, X., Ge, Y., Liao, K., Miao, R., Qiu, X., Koenig, T.K., Chen, S., 2021. Precursors and pathways leading to enhanced secondary organic aerosol formation during severe haze episodes. Environ. Sci. Technol. 55, 15680–15693.
Zhou, L., Zhou, Y., Yao, X., Cai, J., Liu, X., Tang, X., Zhang, Y., Jang, K.S., Jeppesen, E., 2020. Decreasing diversity of rare bacterial subcommunities relates to dissolved organic matter along permafrost thawing gradients. Environ. Int. 134, 105330.